IOPscience iopscience.iop.org

Home Search Collections Journals About Contact us My IOPscience

The dimensionality of ammonium reorientation in $(NH_4)_2S_2O_8$: the view from neutron spectroscopy

This article has been downloaded from IOPscience. Please scroll down to see the full text article.

2008 J. Phys.: Condens. Matter 20 125218

(http://iopscience.iop.org/0953-8984/20/12/125218)

View the table of contents for this issue, or go to the journal homepage for more

Download details:
IP Address: 129.252.86.83
The article was downloaded on 29/05/2010 at 11:10

Please note that terms and conditions apply.

J. Phys.: Condens. Matter **20** (2008) 125218 (11pp) doi:10.1088/0953-8984/20/12/125218

The dimensionality of ammonium reorientation in $(NH_4)_2S_2O_8$: the view from neutron spectroscopy

M Prager[1,2], H Grimm[1], I Natkaniec[3,4], D Nowak[4,5] and T Unruh[6]

[1] Institut für Festkörperforschung, Forschungszentrum Jülich, 52425 Jülich, Germany
[2] Jülich Centre for Neutron Science, Lichtenbergstraße 4, 85747 Garching, Germany
[3] The H Niewodniczanski Institute of Nuclear Physics, 31-342 Krakow, Poland
[4] Frank Laboratory of Neutron Research, Joint Institute of Nuclear Research, 141980 Dubna, Russian Federation
[5] Institute of Physics, Adam Mickiewicz University, 61-614 Poznan, Poland
[6] Forschungneutronenquelle FRM-II, Technische Universität München, Lichtenbergstraße 4, 85747 Garching, Germany

Received 7 November 2007, in final form 8 January 2008
Published 3 March 2008
Online at stacks.iop.org/JPhysCM/20/125218

Abstract
The dynamics of the ammonium ion in ammonium persulfate is studied by inelastic neutron scattering at energy transfers between 0.7 μeV and about 100 meV. NH_4^+ librational modes are clearly split into four energetically different bands, in agreement with the absence of symmetry at the ammonium site. One strong, one medium and two weak hydrogen bonds from the NH_4 ion to neighboring oxygens lead to this unusual potential shape with one dominating overlap matrix elements h_i. Therefore the ammonium dynamics seen by neutron tunneling spectroscopy looks like a rotation about a single axis, that of the strongest hydrogen bond. Quasi-elastic scattering up to $T = 100$ K is dominated by jumps about this specific axis, too. Jumps about the second weak axis modify the quasi-elastic scattering at higher temperature. Results of a previous nuclear magnetic resonance (NMR) quadrupole resonance experiment are consistently interpreted to show the dynamics around the remaining two strong axes. The reduced isotope effect of the lowest librational band is due to a special shape of the potential and not to changes of the hydrogen bond with deuteration.

(Some figures in this article are in colour only in the electronic version)

1. Introduction

Since the early days of molecular spectroscopy, rotational excitations and relaxations have been used as sensitive probes of intermolecular interactions. The data analysis in general is based on the model of single particle rotation, where even complex environments are represented by a simple rotational potential. This potential is calculated from the crystal structure and suitably parametrized intermolecular forces. In the case of ammonium halides the electrostatic interaction was found to dominate the lattice energy. With the octopole moment as the dominant term of an expansion of the charge distribution of the NH_4^+ ion into symmetry adapted functions and point charges at lattice sites, rather accurate *ab initio* rotational potentials were obtained [1]. The symmetries of both the molecule and the environment determine the symmetry of the rotational potential. In the ammonium halides, due to various phase transitions, potentials of tetragonal or cubic symmetry are found. In other materials higher-order terms of an expansion of the rotational potential may be important. In the case of ammonium hexachlorostannate, such terms describe even subtler details of the potential such as the evolution of subminima around the main tetrahedral axes [2].

Most commonly, ammonium rotational potentials are derived from librational energies which are measured either by infrared or neutron spectroscopy [3]. In a similar way the activation energy derived from either NMR spin lattice relaxation measurements or the temperature dependence of quasi-elastic neutron scattering spectra can be used as an input parameter [4]. With the advent of high-resolution

 © 2008 IOP Publishing Ltd Printed in the UK

neutron spectroscopy the tunnel splitting of the ammonium librational ground state of weakly hindered rotors became measurable. On the one hand, the tunnel splitting simply adds a third observable to the refinement problem. More importantly, however, due to its exponential dependence, tunneling represents the most sensitive probe of the strength and symmetry of a rotational potential [5–8] and can lead to a new precision of analysis and therefore a new quality of understanding molecular solids [9, 10].

The theory of rotational tunneling of tetrahedral molecules shows [5] that the rotational ground state is a quintet with nine transitions between the substates which are all energetically different if the site has no local symmetry. With increasing site symmetry, some levels become degenerate. At the highest tetrahedral environmental symmetry, the tunneling spectra are doublets, as in the case of methane or many ammonium salts [8]. On this background, ammoniumpersulfate (APS) is a rather unique material. The tunneling spectrum of the ammonium spherical top measured with neutrons [11] is a single band at an energy transfer of $\hbar\omega_t = 1.12$ μeV. Such a spectrum is characteristic of *one-dimensional* rotation. A very special shape of the ammonium rotational potential is needed to lead to this tunneling spectrum. The environment must show a strongly threefold symmetry, for example by an extraordinarily *strong bond to one proton* and a correspondingly soft potential for rotation about this unique axis. A reminder of the three-dimensional nature of motion may be retained in small splittings between almost degenerate levels. A single-crystal NMR spin lattice relaxation experiment has indeed found a second, much smaller tunnel splitting of $\hbar\omega_t = 0.036$ μeV [12, 13] which cannot be resolved by neutron spectroscopy. A quantitative description of both observations was possible with a potential characterized by one weak barrier with a corresponding large tunnel matrix element and three inequivalent hard axes connected with rather small but different tunnel matrix elements. APS is the only example where such nearly one-dimensional rotation, occasionally predicted from proton NMR spectra for other materials [14], could be confirmed by INS.

Its unique potential shape made APS interesting for further investigations. At first, a crystal structure was established at a sample temperature of $T = 118$ K using x-ray diffraction [15]. The space group $P2_1/c$ of previous studies was confirmed. The site symmetry of the nitrogen is not threefold, as assumed above for simplicity. However, the presence of the shortest hydrogen bond seems indeed to determine a unique rotation axis. The carbon–deuteron4 axis of [15] was identified as the strongest hydrogen bond and a temperature of $T = 25$ K was established below which this axis is fixed on the timescale of the NMR experiment. By including the information from single-crystal deuteron resonance NMR experiments [16–18], the protons were located with an accuracy of 0.01 Å.

Deuteron spin lattice relaxation measurements from a polycrystal [19] and deuteron NMR spectra from a single crystal could be described consistently by a dominantly one-dimensional rotation scaled down by the isotope effect to 0.007 μeV (1.6 MHz). In the experiment the presence of a second one-dimensional tunneling motion at a frequency 4.5 kHz corresponding to a tunnel splitting of 19 peV was also found and interpreted as rotation of the ND_4^+ ion about a second tetrahedral axis. The deuteron NMR resonance experiment has also looked at partially deuterated samples NDH_3^+. At low temperature the deuteron is always localized, since tunneling is only possible in a system of identical particles. Rotation with the D aligned along the strong hydrogen bond was outside the window of the experiment but consistent with a tunnel splitting of 1.12 μeV. Secondary tunneling processes were observed, as in the fully deuterated material, and assigned to one-dimensional rotation of the NH_3 group in the NH_3D isotopomer about the second weak axis. A tunnel splitting of 200 kHz, corresponding to a tunnel splitting of 0.8 neV, was roughly guessed with a significant error. A discrepancy between barrier heights deduced from the deuterated and protonated secondary tunnel splittings was supposed to be due to different multipole moments of the fully and partially deuterated rotor.

The present neutron scattering experiment uses only purely protonated or purely deuterated samples and covers the energy range from 0.7 μeV to 100 meV. This allows us to establish for $(NH_4)_2S_2O_8$ the tunneling splitting and the evolution of the rotational jump dynamics by quasi-elastic scattering. In the regime of lattice modes, the isotope effect is exploited to identify ammonium librations among other lattice phonons. It will be shown that the classical single-particle model can describe consistently all features of ammonium rotational dynamics by a single low-symmetry three-dimensional rotational potential.

2. Theory

2.1. Rotational tunneling

The librational ground state of a tetrahedral rotor represents a quintet state with the totally symmetric A ground state, three states of T symmetry and the highest doubly degenerate E level. At tetrahedral symmetry the T states are degenerate. On lowering the site symmetry, this degeneracy is partly or completely removed [7]. In the pocket state formalism the librational ground state is described by a tunneling matrix [5]. The dominant quantities are the four 120° overlap matrix elements h_i, $i = 1$–4. They determine, in our case, all important features of the energy-level scheme. After block diagonalization, four identical 3×3 submatrices are formed whose eigenvalues represent the three T levels. We are interested in the present work in ammonium groups with one distinguished rotation axis. The full problem with four different h_i is solved in [12] following [6]. At our energy resolution the essence of the problem is already contained in the simpler case of a threefold site symmetry. In this case, only two different overlap matrix elements exist and the five eigen-energies of the librational ground state are

$$\begin{aligned} E_{\mathrm{A}} &= 2h_1 + 6h_2 \\ E_{T_1} &= 2h_1 - 2h_2 \\ E_{T_2} &= E_{T_3} = -h_1 + h_2 \\ E_{\mathrm{E}} &= -h_1 - 3h_2. \end{aligned} \tag{1}$$

Overlap matrix elements h_i are negative. It is obvious that in the case of $h_2 = 0$, which characterizes the presence of one exceedingly strong hydrogen bond, T levels merge with A- and E-levels, respectively, to form a doublet separated by $3h_1$ with a twofold degenerate ground state and a fourfold degenerate excited state. Such a doublet represents exactly the level scheme of a one-dimensional rotor. For finite small h_2 the tunneling groundstate splits by 2Δ and the excited state by Δ, with $\Delta = 4h_2 \ll 3h_1$.

The neutron scattering function of a tetrahedral rotor in the outlined limit $h_2 \ll h_1$ can be obtained from tables A.2a and A.3a of [7], which summarizes the results of [6] and is

$$S^{\mathrm{tun}}_{3\mathrm{d}}(Q,\omega) = \tfrac{2}{3}\{(4 + 2j_0(Qd))\delta(\omega) + (1 - j_0(Qd))[\delta(\omega - \omega_t) + \delta(\omega + \omega_t)]\}. \quad (2)$$

The intensity is normalized to the scattering of one proton. Q is the momentum transfer, d the proton–proton distance and j_0 the spherical Bessel function of zeroth order. This scattering function is identical to that of a one-dimensional threefold rotor with the additional elastic scattering from the fixed fourth proton.

If a rotational potential can be calculated from intermolecular interaction and the crystal structure, the values of the overlap matrix elements h_i, which are free parameters in a phenomenological approach, will be fully determined *ab initio*. Such a comparison between experiment and theory actually represents the most sensitive test of force fields.

2.2. Jump reorientation

At higher temperature, a time-dependent environment destroys the quantum description. Instead of inelastic transition bands, quasi-elastic scattering is observed as the response of classical stochastic dynamics. The jump rotation of a tetrahedron in a low-symmetry environment can be related to a complex scattering function composed of a number of Lorentzians of different widths [20–22]. The models used in the following are only phenomenological, however, and are based on distinct jump rates around inequivalent rotation axes.

The scattering function of one-dimensional reorientation of a tetrahedron about a fixed threefold axis [4], including the elastic scattering of the proton on the axis, reads

$$S^{\mathrm{qns}}_{1\mathrm{d}}(Q,\omega) = 2(1 + j_0(Qd))\delta(\omega) + 2(1 - j_0(Qd))L(\omega,\Gamma). \quad (3)$$

The width $\Gamma = \frac{3}{2}\nu$ of the Lorentzian L is determined by the jump rate ν and is related to the rotational barrier by an Arrhenius dependence:

$$\Gamma(T) = \Gamma_0 \exp\left(-\frac{E_\mathrm{a}}{kT}\right). \quad (4)$$

The temperature dependence of quasi-elastic scattering thus allows us to obtain the activation energy E_a and, therefore, under certain assumptions, a rotational potential.

Quasi-elastic scattering of tetrahedra reorienting about all four threefold axes with identical rates ν (tetrahedral site symmetry) is also represented by a single Lorentzian [23] and a linewidth $\Gamma = \frac{4}{3}\nu$:

$$S^{\mathrm{qns}}_{3\mathrm{d}}(Q,\omega) = (1 + 3j_0(Qd))\delta(\omega) + 3(1 - j_0(Qd))L(\omega,\Gamma). \quad (5)$$

At lower site symmetries the scattering function becomes a superposition of a few quasi-elastic Lorentzians with linewidths determined by different combinations of the different jump rates about the different inequivalent threefold axes. For our purpose, the case with a second somewhat soft axis and two hard rotation axes is interesting. From the four jump rates, the two about the hard axes shall be neglected. This generalization with respect to the seminal paper [23] leads to a 4×4 jump matrix J

$$J = \begin{pmatrix} -2\nu_2 & 0 & \nu_2 & \nu_2 \\ 0 & -2\nu_1 & \nu_1 & \nu_1 \\ \nu_2 & \nu_1 & -2(\nu_1+\nu_2) & \nu_1+\nu_2 \\ \nu_2 & \nu_1 & \nu_1+\nu_2 & -2(\nu_1+\nu_2) \end{pmatrix} \quad (6)$$

with eigenvalues

$$E_0 = 0$$
$$E_1 = 3h(\nu_1 + \nu_2) \quad (7)$$
$$E_{2/3} = \tfrac{3}{2}h(\nu_1 + \nu_2) \pm \tfrac{1}{2}h\left(9(\nu_1^2 + \nu_2^2) - 14\nu_1\nu_2\right)^{0.5}.$$

At low temperatures, eigenvalues E_1 and E_2 determine a doubly degenerate quasi-elastic line whose width is only determined by the fast jump rate ν_1, while the line assigned to E_3 merges with the elastic line. With increasing temperature, E_3 increases and a second narrower and weaker component emerges from the elastic line. An expansion of the eigenvalues for small ν_2 shows that the width of this narrow component is proportional to ν_2. With increasing ν_2, the degenerate broad component decomposes smoothly into two components of different widths.

If only elastic intensity is measured as a function of sample temperature, a loss of intensity is observed when a quasi-elastic component becomes comparable to the instrumental energy resolution. The intensity drop has an *atan* shape and its height is determined by the elastic incoherent structure factor EISF at the momentum transfer Q that is used [24]:

$$I(Q,T) = \mathrm{DWF}(Q)\left\{\mathrm{EISF}(Q) - (1 - \mathrm{EISF}(Q))\frac{1}{\pi}\left(\mathrm{atan}\left(\frac{\delta E_\mathrm{res}}{\Gamma(T)}\right)\right)\right\}. \quad (8)$$

$T_{1/2}$ is the temperature where half of the quasi-elastic intensity has left the elastic window. The linewidth $\Gamma(T_{1/2})$ is equal to δE_res. With this knowledge, and postulating a reasonable value of Γ_0, one can derive an activation energy E_a from the Arrhenius law equation (4).

In the case of an inelastic fixed window scan, the intensity is measured at an offset energy ΔE as a function of sample temperature. This intensity is zero at low temperature. The intensity becomes a maximum at T_max where the quasielastic linewidth becomes equal to the an offset energy ΔE. Thereafter the intensity decreases again. This is a similar

relation to the one for the elastic fixed window scan and can also be used to derive an activation energy. The inelastic fixed window is more sensitive, since no spurious elastic scattering is superimposed on the behavior of the quasi-elastic component. On the other hand, this disables a calibration of the total intensity and prevents a straightforward determination of the EISF. The relative intensities of multiple components of a spectrum are precisely reproduced, however.

2.3. Density of states

The lattice modes of a polycrystalline material at low temperature (system energy gain only) are contained in a scattering function [25]

$$S_{\mathrm{DOS}}(Q,\omega) \sim \sum_j \sigma_j \frac{1}{2M_j} \mathrm{DWF} \frac{Q^2\langle u_j^2\rangle}{\omega_j} \times \delta(\omega - \omega_j(q)). \quad (9)$$

The intensity of a mode is proportional to the scattering cross section σ_j of the atoms of mass M_j moving with mean square amplitude $\langle u_j^2\rangle$ in the eigenmode of energy $\hbar\omega_j$. DWF is a global Debye–Waller factor. Hydrogen has one of the largest scattering cross sections. Therefore eigenmodes involving hydrogen with large amplitude displacements $\langle u\rangle$ dominate the spectra in protonated materials. In case of rotational modes of molecular systems, the effect of the mass has to be replaced by that of the square root of the momentum of inertia. The corresponding isotope effect is especially large, $\sqrt{2}$ in harmonic approximation, and allows, if observed, identification of ammonium librations.

3. Experiments and results

The protonated material was bought from the Aldrich company and was used in the experiment without further treatment. The deuterated material was prepared by H Zimmermann of the molecular crystal group at the Max-Planck Institute for Medical Research, Heidelberg, by repeated recrystallization of isotopically normal APS from a solution of D_2O (99.8%). The single crystal from the final solution had well developed natural-growth planes. Pieces remaining after cutting out an oriented crystal for a neutron diffraction experiment were crunched to a powder and used for neutron spectroscopy.

Experiments were performed at various spectrometers in a wide range of transition energies. The inverse time-of-flight spectrometer NERA [26] of the pulsed reactor IBR-2 in Dubna, Russia, was used for energy transfers from a few meV to ∼200 meV. Due to the inverse geometry, the spectrometer also yields diffraction patterns of the sample. At improved energy resolution and lower sample temperature, the hybrid thermal time-of-flight spectrometer SV29 [27] at Forschungszentrum Jülich, Germany, was used. In the energy range ±17 μeV and a corresponding energy resolution $\delta E_{\mathrm{res}} = 0.99$ μeV, spectra were obtained using the backscattering spectrometer BSS [28] of Forschungszentrum Jülich with its standard Si(111) monochromator. Sample temperatures were $T = 4.5$–120 K. Above this temperature the offset configuration of the spectrometer with an offset energy of 14 μeV was used to follow further the evolution of quasi-elastic spectra in the energy range $-31\ \mu\mathrm{eV} \leqslant E(\mu\mathrm{eV}) \leqslant 3\ \mu\mathrm{eV}$. In both setups, integral dynamical information was obtained from fixed window scans. At an improved energy resolution of 0.7 μeV, some spectra were re-measured at the new SPHERES backscattering spectrometer of the Jülich Centre for Neutron Science at FRM2, Munich [29]. At a reduced energy resolution $\delta E_{\mathrm{res}} = 40$ μeV, a set of first quasi-elastic spectra was measured at the high-resolution time-of-flight (TOF) spectrometer NEAT [30] of Hahn-Meitner Institute, Berlin. Final quasi-elastic spectra were measured in an extended temperature regime and with improved energy resolution of $\delta E_{\mathrm{res}} = 30$ μeV at the TOFTOF cold TOF spectrometer [31, 32] at FRM2, Munich, using a wavelength of 6.5 Å. From all spectra, a measured background is subtracted before mathematical treatment. The theory function is in all cases convoluted numerically with the measured (vanadium) resolution function.

3.1. Crystal structure

The diffraction data obtained by NERA do not have the quality and range to allow a full structure analysis but can be used to test consistency with published structures. Since the experiment was performed at much lower temperature than the x-ray structure determination [15], we have refined the lattice parameters and angles and the nitrogen–proton distances within the space group $P2_1/c$ using dedicated software [33]. The two structure determinations compare in the following way. At $T = 21(118)$ K, the unit cell parameters are $a = 6.1281(6.1340)$ Å, $b = 7.8948(7.9324)$ Å, $c = 7.6385(7.7541)$ Å, $\beta = 94.69(94.966)°$, and $V = 368.31(375.88)$ Å^3. The accuracy of the lattice parameters is ±0.0003 Å. While the overall agreement of positions of Bragg lines becomes rather good this way, there are qualitative deficiencies. Bragg peaks are clearly observed which should *not* be present in the $P2_1/c$ space group. For example, a strong (101) peak contradicts the condition that $(h0l)$ reflections are only allowed with $l = 2n$. An earlier attempt to solve the low-temperature structure at $T = 5$ K by single-crystal neutron diffraction failed [34] due to a twinning of the crystal. The present data show that the structure at He temperature is likely slightly different from the one at $T = 118$ K [15].

Another important observation is that some Bragg lines observed in the deuterated sample are absent in the protonated material. If this is not due to accidentally vanishing structure factors, the two materials may crystallize in different space groups but with rather similar lattice parameters (figure 1) since Bragg lines of the protonated material find their counterpart in the deuterated sample at almost identical momentum transfer.

It is not unusual in systems with hydrogen bonds that deuteration leads to different phase behavior. Examples are given by the ammonium hexahalo metallates [35–37] and classical hydrogen bonded systems [38]. The theory of second-order phase transitions then predicts a critical slowing down of the mode driving the phase transition. Thus, parts of the lattice dynamics change in an extraordinary way and systematics based on pure isotope effects is often violated. In the case

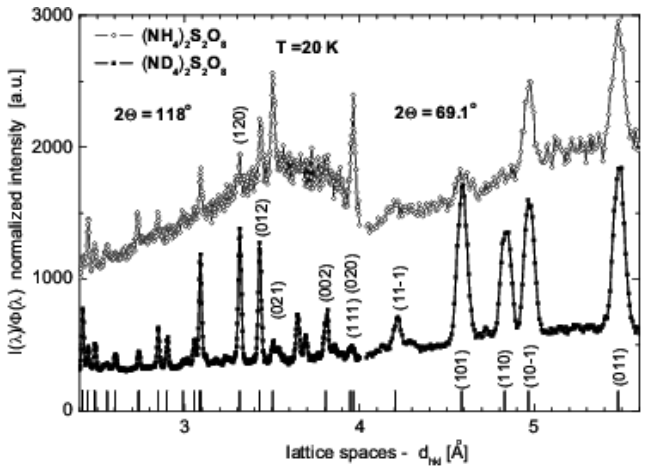

Figure 1. Diffractograms of protonated (upper line) and deuterated (lower line) ammonium persulfate. Samples temperatures $T = 20$ K. Spectrometer: Nera, Dubna

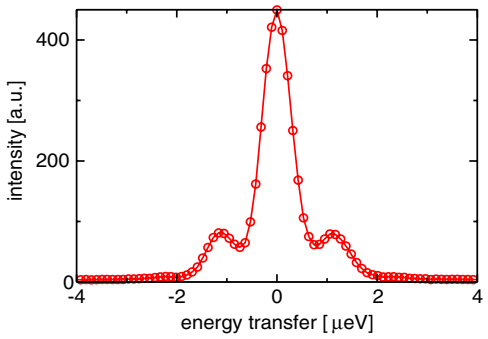

Figure 2. High-resolution tunneling spectrum of $(NH_4)_2S_2O_8$. Sample temperature $T = 4.5$ K. $Q = 1.4$ Å^{-1}. Spectrometer: SPHERES, JCNS. Solid line: fit.

of the ammonium hexahalo metallates the characteristic soft mode is a libration of the NH_4^+ ion leading to the orthorhombic distortion of the original cubic lattice [39].

3.2. High-resolution neutron spectra

A tunneling spectrum and selected quasi-elastic spectra are shown in figures 2–5. The improved energy resolution of the new backscattering spectrometer SPHERES compared to BSS was necessary to fully resolve the tunneling transition (figure 2). To reduce multiple scattering we used a flat sample with a calculated scattering probability of about 12%. As expected, only a little intensity is found at twice the tunneling energy. Such bands were rather strong in a previous experiment and must be assigned to multiple scattering due to the use of a sample that is too thick [11]. A fit of the spectrum by three resolution functions with all parameters left free yields a tunnel splitting of (1.09 ± 0.04) μeV, in good agreement with 1.12 μeV from the previous experiment [11]. Spectra are summed up in an angular range $(90 \pm 15)^\circ$ corresponding to an average momentum transfer of the spectrum of $Q = (1.40 \pm 0.18)$ Å^{-1}. The fitted intensities reproduce almost exactly the ratio of elastic and inelastic intensities of the scattering

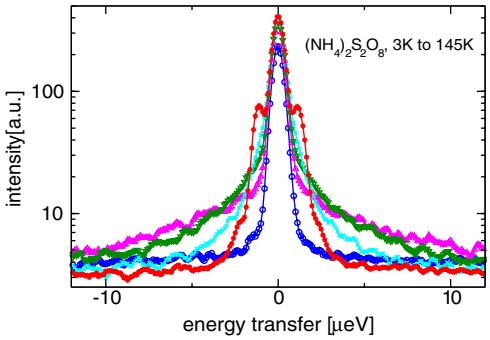

Figure 3. Temperature evolution of high-resolution spectra of $(NH_4)_2S_2O_8$ from $T = 3$ K (***) via 50 ($\times\ \times\ \times$), 58 ($\triangledown$), 67 ($\triangle$) to $T = 145$ K ($\circ\ \circ\ \circ$). $Q = 1.4$ Å^{-1}. Spectrometer: SPHERES, JCNS.

Table 1. Quasi-elastic linewidths of ammonium persulfate. Spectrometers used: BSS for $T \leqslant 90.2$ K, TOFTOF for $T \geqslant 70$ K.

BSS		TOFTOF	
T (K)	Γ (μeV)	T (K)	Γ (μeV)
50.7	0.66	70	6.23
55.6	1.35	80	16.6
60.5	2.48	90	30.4
65.5	4.36	100	47.9
70.4	6.32	120	90
75.4	8.23	140	203/47
80.3	9.95/0.19	160	294/71
85.3	12.3/0.51	180	384/112
90.2	15.1/0.90	200	472/167
		220	550/241
		240	691/312
		270	999/404
		290	1222/470

function equation (2). The increased elastic intensity from the fixed proton is, besides the single tunneling peak, a second independent confirmation of near to one-dimensional rotation.

The evolution with temperature is shown in figure 3. The spectra that are presented were recorded while the sample temperature was lowered continuously from 145 to 2.6 K during 24 h. To obtain sufficient statistics, data from a rather broad temperature interval had to be summed up. This prevents a quantitative analysis. Inelastic tunneling intensity is visible in the spectra up to a sample temperature $T \sim 45$ K. Above $T \sim 50$ K the scattering is quasi-elastic and in qualitative agreement with results from the previous experiment on BSS taken at a constant temperature. Between $T \sim 50$ and 70 K the spectra can be fitted well by a superposition of an elastic delta function and a single quasi-elastic Lorentzian convoluted with the resolution function (figure 4, solid lines). The quasi-elastic line represents jump reorientation about the axis of the three-dimensional rotational potential function with the lowest barrier. In agreement with the scattering function for one-dimensional rotors, the quasi-elastic component contains three times the intensity of the tunneling band of figure 2. The ratio of elastic to inelastic intensities turns out to be almost independent of sample temperature and is consistent with the value required for the average momentum transfer, $Q = 1.6$ Å^{-1}, by the scattering function equation (3).

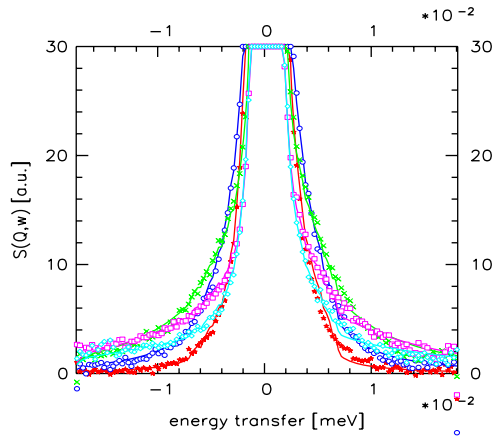

Figure 4. Quasi-elastic spectra of $(NH_4)_2S_2O_8$. Temperatures: 50 K ($\star$), 55 K ($\circ$), 60 K ($\times\times\times$), 65 K ($\square$), 70 K ($\diamond$). Momentum transfer $Q = 1.6$ Å^{-1}. Instrument: BSS of FZJ. Solid lines: fits.

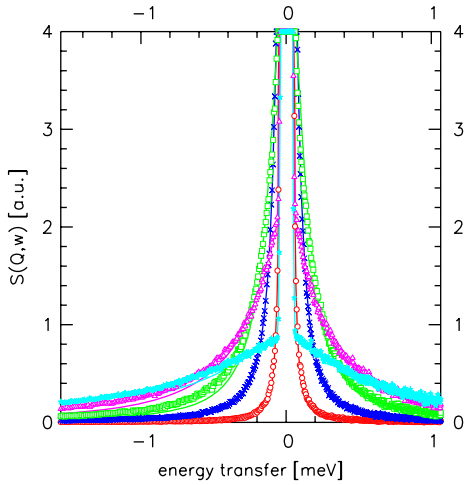

Figure 5. Quasi-elastic spectra of $(NH_4)_2S_2O_8$. Temperatures: 70 K ($\circ$), 100 K (xxx), 160 K ($\square$), 220 K ($\triangle$), 290 K ($\diamond$). Instrument: TOFTOF of FRM2, $\lambda = 6.5$ Å. Elastic momentum transfer $Q = 1.4$ Å^{-1}. Solid lines: fits.

Between $T = 80$ and 100 K, a second quasi-elastic Lorentzian is needed to model the quasi-elastic intensity. We assume that rotation about the next soft axis becomes observable. According to the eigenvalues of equation (7), the intensity of this second component is half that of the broad line and thus reproduces the degeneracies.

If measured with reduced energy resolution on a TOF spectrometer (figure 5), the narrow component is invisible until higher temperatures and a single quasi-elastic Lorentzian fits the spectra very well up to $T = 100$ K. Due to an overlap with the density of states, the fit range is restricted from -0.5 to $+1.0$ meV. Only for $T \geqslant 140$ K, a description with two Lorentzians of different widths and the intensity ratio 2:1, already found in the BSS spectra, becomes essential for a good description. These are the characteristics of the scattering function based on the jump matrix equation (6) in a regime where the two broad components are still indistinguishable. The Q-dependence of the intensities again

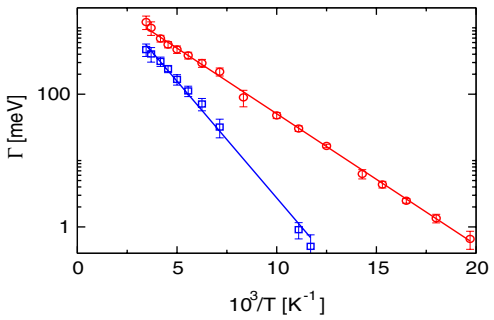

Figure 6. Arrhenius presentation of the quasi-elastic linewidths at temperatures 50 K $\leqslant T$(K) $\leqslant$ 250 K. Solid lines: fits. For details, see the text.

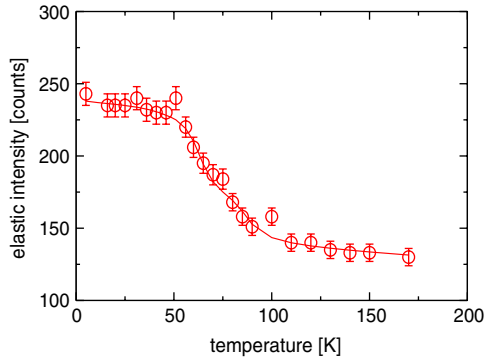

Figure 7. Elastic fixed window scan on $(NH_4)_2S_2O_8$. Instrument: BSS of FZJ. Energy resolution $\delta E = 0.99$ μeV. Average momentum transfer $Q \sim 1.6$ Å^{-1}.

confirms both processes as molecular reorientations. The more the widths of the two Lorentzians approach each other, the more this assumption is violated. Figure 6 shows that the temperature dependence of the linewidths of the two quasi-elastic components (table 1) can be described by two Arrhenius functions over the full temperature range 50 K $\leqslant T$(K) $\leqslant$ 290 K. Weak deviations appear at the highest temperatures. The reason for the larger systematic error bars at high temperatures lies in the conditions imposed. On the other hand, an unrestricted fit is not successful, since quasi-elastic lines extending into the regime of phonons risk being abused to contribute to modeling of the phonon density of states. Activation energies $E_a^1 = 40$ meV and $E_a^2 = 71$ meV are obtained with prefactors $\Gamma_0^1 = 4.8$ meV and $\Gamma_0^2 = 9.0$ meV.

An elastic fixed window scan is constructed from the BSS spectra based on the fitted and normalized pure elastic intensities. This plot (figure 7) shows a step at a temperature where the quasi-elastic component in the spectrum becomes broader than the energy resolution $\delta E_{res} = 0.99$ μeV of the spectrometer. This step spreads over a temperature range which is too wide for a single dynamical process. Therefore, and based on the analysis of the time-of-flight spectra and the inelastic fixed window—see below—we forced the curve to contain two components of type equation (8) with relative intensities 2:1 (solid line of figure 7). Fixing the prefactors to the values $\Gamma_0 = 4.8(9.0)$ meV deduced from the

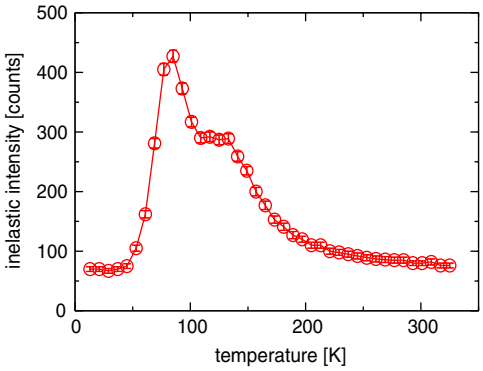

Figure 8. Inelastic fixed window scan on $(NH_4)_2S_2O_8$. Instrument: BSS of FZJ. Offset 14 μeV. Energy resolution $\delta E = 1.56$ μeV. Momentum transfer $Q \sim 1.8$ Å^{-1}.

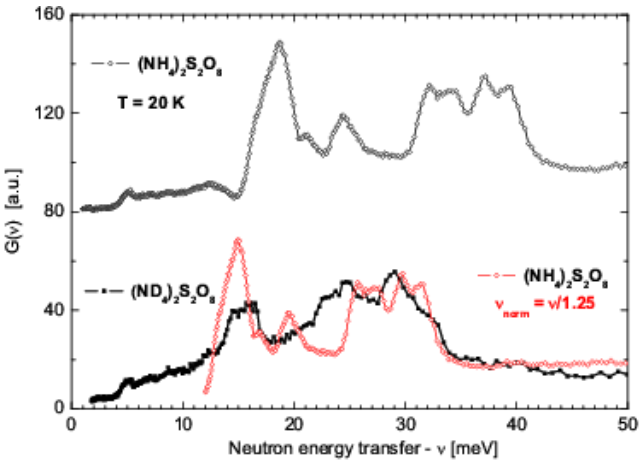

Figure 9. Inelastic spectra of ammonium persulfate: protonated (top), deuterated (bottom, □), protonated scaled by a factor 1.25 (bottom, ○). Sample temperatures $T = 21$ K. Spectrometer: NERA, Dubna.

quasi-elastic neutron scattering (QNS) fit activation energies $E_a = 46(71)$ meV are derived. The difference with the results from the analysis of complete spectra is a measure of the accuracy of the integral fixed window method. For the respective components, half of their intensity has left the elastic window at temperatures $T_{1/2} = 63$ and 87 K. The smaller activation energy is in the simple model of a one-dimensional $\cos 3\varphi$ potential well consistent with both the tunnel splitting and the low-energy librational mode (see below).

The smooth decrease in the integrated intensity with temperature allows us to determine the Debye–Waller factor in equation (8) and there from [40] a mean square displacement $\langle u_0^2 \rangle = (0.038 \pm 0.01)$ Å^2 or $\langle u_0 \rangle = (0.20 \pm 0.03)$ Å. This value has to be compared with the angular width $\langle \varphi_0 \rangle$ of the ground-state wavefunction of the Schrödinger equation, as determined by the measured tunnel splitting. With $\langle \varphi_0 \rangle = \pm 29°$ and a nitrogen–hydrogen distance of $r_{NH} = 1.04$ Å, one gets $r_{NH} \langle \varphi_0 \rangle = \pm 0.17$ Å full width half maximum (FWHM), which is in reasonable agreement with $\langle u_0 \rangle$.

Using the offset monochromator of the BSS spectrometer we can measure the spectral density at an energy transfer of 14 μeV with an energy resolution of 1.56 μeV. Figure 8 shows original data which still contain a flat sample-independent instrumental background. From the elastic fixed window scan we expect a linewidth of the broad component of 14 μeV around $T = 85$ K. At this temperature we indeed observe the first maximum in the offset fixed window scan (figure 8), which is therefore related to jump reorientation of ammonium tetrahedra about the strong hydrogen bond. A new and unusual observation is the appearance of a second maximum. The position of the maximum is in full agreement with the narrower and weaker quasi-elastic component of figure 6 reaching the width of the offset energy $\Delta E = 14$ μeV at $T_{1/2} = 125$ K for $\Gamma_0 = 9$ meV and the activation energy of $E_a \sim 71$ meV. Its intensity is close to half that of the main component.

While rotational tunneling spectroscopy supposed a one-dimensional rotation of the ammonium ion, quasi-elastic spectra have shown rotation about a second axis. This shows that sensitivity also has disadvantages. The exponential reduction of the overlap matrix elements leads to an exponential reduction of some splittings in the ground-state tunnel multiplet. Already at a factor of 1.5 difference between the heights of the saddle points of the three-dimensional potential, the higher barriers no longer affect the tunnel spectrum at the best energy resolution of neutron spectroscopy. In quasi-elastic scattering, the temperature can counteract the effect of an increased barrier height, such that jumps around harder axes become visible and reveal the three-dimensional character of motion.

Table 2. Characteristic energies observed in ammonium (A) persulfate.

	Transition energies (meV)		
Mode assignment	Protonated sample	Deuterated sample	Isotope effect
A-tunneling	0.00109	—	
Acoustic phonons	5.1	5.1	
Acoustic phonons	12.5		
A-libration 1	16.5	14.0	1.18
A-libration 1	18.0	15.5	1.16
A-libration 2	21.2	15.5	1.37
A-libration 2	24.4	17.5	1.38
A-libration 3	32.2	24	1.34
A-libration 3	34.1	24.8	1.38
A-libration 4	37.2	29.2	1.27
A-libration 4	39.3	31.4	1.25
Internal mode	50	53.4	
Internal mode	61		
Internal mode	71	95.2	

3.3. Phonons

The largest energy range is covered by the NERA spectrometer. The energies of the observed vibrational bands (figure 9) are shown in table 2 for both the protonated and the deuterated samples. A strong shift to lower energies with deuteration is observed for all strong bands of $(NH_4)_2S_2O_8$. The low-energy part of the spectrum was measured with somewhat improved energy resolution and a temperature $T = 2.3$ K on SV29. In the protonated sample the band around 18.5 meV is confirmed to represent a still unresolved doublet which is shifted to a

Table 3. One-dimensional potentials V_3 derived from the *bold* input parameters. Dependent quantities are shown in standard figures. nFW: neutron fixed window. NMR-Q: nuclear quadrupolar resonance. NMR-T_1: spin lattice relaxation. D/H: deuterated/hydrogenated rotor. The very small tunnel splittings of the two lowest lines are obtained from an asymptotically valid formula for strong potentials [43]. Results from deuterated samples are scaled to the protonated material by keeping the potential strength constant. Top to bottom: axes of rotation with increasing barrier. $B_{NH_4} = 0.722$ meV from [15].

Technique/ reference	$2V_3$ (meV)	$\hbar\omega_t$ (μeV)	E_{01} (meV)	E_a (meV)	Remark
INS	57	**1.09**	17.4	48	
INS	56	1.12	**17.3**	47	
e-nFW	55	1.25	17.1	**46**	$T_{1/2} = 63$ K, equation (8)
QNS	47	2.7	15.6	**40**	
i-nFW	50	2.0	16.2	**41**	$T_{1/2} = 85$ K, equation (8)
NMR-T_1 [15]	50	2.0	16.2	**41**	D
NMR-Q [16]	57	**0.007**(1.6 MHz)	12.7	50	D
	57	1.09	17.4	48	scaled to H
NMR-Q [16]	101	$\mathbf{1.9 \times 10^{-5}}$ (4.5 kHz)	17.3	92	D in ND_4
	101	0.03	23.9	88	scaled to H
NMR-T_1 [12]	110	**0.018(8.7 MHz)**	25.0	97	H
NMR-T_1 [15]	90	0.0001	16.2	**82**	D
	90	0.07	22.4	78	scaled to H
QNS	82	0.13	21.3	**71**	
INS	105	0.025	**24.4**	92	
e-nFW	79	0.17	20.9	**68**	
i-nFW	81	0.14	21.2	**70**	
INS	188	0.007	**33.2**	171	
INS	245	0.0008	**38.2**	225	
NMR-Q [16]	245	**0.0008(200 kHz)**	38.2	225	H in NH_3D

mean energy of 15 meV in the deuterated sample. Using the shorter wavelength $\lambda = 1.17$ Å at SV29, the unresolved wing of the deuterated sample around 30 meV in the Nera spectrum is clearly resolved as a doublet due to the improving energy resolution with energy transfers of a direct TOF spectrometer.

In a first step, the mode assignment in table 2 is based on the isotope effect and focused to identify the ammonium librations. In harmonic approximation, an isotopic shift by $\sqrt{2}$ is expected. In our case, different isotopic shifts of the four librational modes are found from table 2. This could, as in other hydrogen-bonded systems be explained by the assumption that deuteration changes the properties of the hydrogen bonds and therewith the ammonium rotational potential. We will show in the discussion that such an unproven ad hoc hypothesis is not needed to understand the deviation from a harmonic isotope effect. The dominant intensity from librational modes in neutron spectra following from equation (9) from the large scattering cross section σ_H of hydrogen and the large mean-square amplitude $\langle u_H \rangle^2$ in the anharmonic rotational potential is taken as a second characteristic property of librational modes to confirm the assignment. As a consequence of mode-specific isotopic shifts, the two lowest librational bands almost overlap in the deuterated compound.

The four different librational energies of table 2 characterize the four different rotational barriers about the four tetrahedral axes of the molecule. In agreement with the lack of symmetry, they are all different. The two lowest bands show energies expected from the barriers deduced from tunneling and quasi-elastic scattering and are therefore related to the same rotational barrier. Two modes are at such high energies (>30 meV) that jumps about the corresponding axes can be neglected at all temperatures studied in the present work. They may be seen by NMR techniques, however (see below). The separation of the two hard rotation axes from the two softer ones is *a posteriori* the justification of the jump model used to interpret the quasi-elastic spectra of this work and the frequency-dependent spin lattice relaxation with their two tunnel matrix elements [12].

The four librational energies are due to the different strengths of the four hydrogen bonds. To explain the observed librational energies, one strong hydrogen bond, the one keeping the ammonium molecule oriented, a somewhat weaker one and two really weak ones are required. The crystallographic study of the environment of the ammonium ion came to exactly the same conclusion [15].

A surprising feature is that the two high-energy librational modes are doublets. At these large energies, a coupling to lattice modes with corresponding dispersion is unlikely. Thus this splitting could be a fingerprint of a more complex potential shape eventually with subminima around the tetrahedral molecular axes.

4. Discussion

The discussion aims at a consistent qualitative explanation of the ammonium dynamics in the three-dimensional rotational potential. For quantitative estimates we use one-dimensional projections of this potential corresponding to rotations about the four tetrahedral axes. We base the analysis on the measured independent parameters shown in bold face in table 3. From each observable, a height V_3 of a purely threefold one-

dimensional rotational potential

$$V(\varphi) = \frac{V_3}{2}(1 - \cos(3\varphi)) \tag{10}$$

is derived from the solution of the Mathieu equation [7, 8]. The program written for this purpose follows the matrix formalism outlined in [41]. Other eigen-energies of the rotor in this potential such as the first excited librational mode E_{01}, the ground-state tunnel splitting $\hbar\omega_t$ and finally the activation energy E_a are shown. They make the connection to techniques with the respective observables. The assumption of a pure $\cos(3\varphi)$ potential is, despite being believed to be a good one, a simplification which obviously must lead to some deviation of calculated eigen-energies from observed values. One can only expect to find the calculated modes or saddle points in the *right range*. In a second step, a refinement of the shape of the—still one-dimensional—potential is considered to improve consistency. For this purpose, equation (10) is extended by including higher-order terms to the ground term of the Fourier expansion equation (10).

If results from a deuterated sample are considered, as in the case of NMR deuteron quadrupole resonance experiments, we assume that the absolute rotational potential is the same in both the protonated and the deuterated materials and we then obtain the characteristic energies of the NH_4^+ ion just by scaling with the rotational constant in the Mathieu equation. While such a comparison would be completely appropriate and is generally used for high-energy internal vibrational modes, it leads to valid eigen-energies of low-energy librational modes only if the rotational potentials in the protonated and the deuterated material are really identical. If the environment changes—and, in the case of strong hydrogen bonds, deuteration can be such a critical change—deviations from this standard behavior may be observed. Therefore a complete agreement of results scaled to the hydrogenated material from experiments with deuterated samples with those measured directly with protonated samples cannot be expected. In $(NH_4)_2S_2O_8$, at first glance the lowest librational mode looks to be affected by this problem.

The information in table 3 is organized such that dynamics around similar rotational barriers, and thus occurring on the same timescale, are blocked in separate sections. The largest number of observations is related to the two weak barriers.

It seems to fit nicely with the general experience that the observed ground-state tunnel splitting of 1.09 μeV (1.12 μeV in [11]) and the lowest librational mode at 17.3 meV can be almost perfectly explained by a one-dimensional potential $V_3 \sim 57$ meV [8]. However, the threefold model potential cannot explain simultaneously the excessively low mean activation energy. Therefore we have tried to adjust a more complex potential containing a sixfold term. A sixfold term V_6 added under the condition of keeping the tunnel splitting constant by a corresponding change of V_3 has the following effects: if its sign is positive, then one gets an increase in the librational energy and a decrease of the activation energy, while the opposite changes are found for negative V_6. In our case, a potential which describes simultaneously the tunnel splitting and the activation energy E_a measured directly by quasi-elastic neutron scattering and/or the NMR-T_1 experiment with the deuterated sample [15] is reached for a dominant V_6 term. Then, however, an excessively high librational mode at about 20 meV is calculated. At this stage we have to keep in mind that, for a dominatant sixfold potential, the next higher Fourier term, V_9, can no longer be neglected. Indeed, a potential describing all observed quantities can be found this way: $(V_3, V_6, V_9) = (24\text{ meV}, 56\text{ meV}, -10\text{ meV})$. We should not put too much trust in the numbers, since the model of one-dimensional rotation is an approximation. However, this solution has a very interesting new aspect: in this potential the isotope effect no longer follows the prediction of a harmonic system. While it has weakened a little bit for the tunneling splitting and also leads to an increase in the activation energy due to the lowering of the ground state in the potential, it has become very small for the librational mode. This means, in our opinion, that the observed reduced *isotope effect of the lowest librational mode is the consequence of the unusual shape of the rotational potential* and *not* a result of a change in the properties of the hydrogen bond with deuteration.

The small tunnel splittings and the long characteristic times observed in various NMR experiments have been [16], and can be, assigned to the dynamics around the next harder axis. The normal size of the isotope effect of this mode shows that here the rotational potential has essentially the threefold symmetry of the rotor. Scaling the results obtained for deuterated samples to protonated materials under the assumption that the rotational potential is the same in both isotopic species adds a tunnel splitting to the parameters determining the rotational potential. A look at table 3 shows that, on the basis of a pure V_3 potential, the NMR experiment yields a systematically higher barrier. The librational mode of the inelastic neutron scattering (INS) spectrum leads to a rather similar amplitude, however. We try again to reconcile the three observables by adding a weak sixfold term. The best agreement is obtained for $(V_3; V_6) = (83\text{ meV}; 9\text{ meV})$ with $\hbar\omega_t = 0.07$ μeV, $E_{01} = 24.5$ meV and $E_a = 70$ meV. To our mind, the largest error is on the scaled tunnel splitting. Therefore the largest deviation was allowed for $\hbar\omega_t$. However, even this error is only about a factor of three.

One extremely slow process (200 kHz) was observed for NH_3D^+ ions by NMR quadrupole resonance [16]. The assignment to a H_3 permutation with the deuteron fixed to the second strongest hydrogen bond led to an isotope effect that is inconsistent with the same dynamical process: tunneling about the second weak axis, observed for ND_4^+. The two barriers estimated along the same arguments differed by ~50%. Such a difference slows down the tunneling process by orders of magnitude. The authors argued that the different electrical properties of these two ammonium isomers—NH_3D has a dipole moment; ND_4 not—lead to significantly different rotational potentials. The argument was not outlined quantitatively and thus remains an unproven suggestion. The inconsistency can be removed, however, without special assumptions if we consider rotation about so far neglected axes, in the same way as above. The barrier heights about the two hardest axes of rotation (the lowest lines of table 3) are most clearly determined from the librational

modes observed in high-energy inelastic neutron spectra. On the basis of the large isotope effect, we clearly identify the modes between 33 and 38 meV as NH_4^+ librations (table 2). For a pure $\cos(3\varphi)$ potential we derive barrier heights of $V_3 = 188$ meV and 245 meV, respectively (within the limits of the one-dimensional model used). A corresponding tunnel splitting of the librational ground state is very small but still *in the range of* NMR spectroscopy. Since the overlap of the molecular wavefunctions and hence the tunnel splitting cannot be reliably calculated for such strong potentials by the matrix diagonalization program, we use the analytical expression derived for strong one-dimensional potentials [42, 43]:

$$\ln\left(\frac{\hbar\omega_t}{B}\right) = -\alpha\sqrt{\frac{V_3}{B}} + \beta. \tag{11}$$

The energies are given in units of the rotational constant B. The values α and β depend on the shape of the potential. Here we use average values $\alpha = 0.95$ and $\beta = 4.1$. For the outlined potentials, equation (11) yields $\hbar\omega_t = 0.007$ and 0.0008 μeV. These more precise tunnel splittings are larger than those of the diagonalizing procedure with a Hamiltonian matrix of range 21. It is obvious that the NMR quadrupole resonance result [16] fits nicely into this scheme. No *ad hoc* hypothesis on charge redistribution in partially deuterated ammonium ions is needed.

The weak point in our discussion is the restriction to a superposition of four one-dimensional reorientational processes for reasons of mathematical feasibility. Instead, a full three-dimensional model should be used which may take into account an eventual deviation of the spherical top towards a distorted tetrahedron, as already supposed by the reduced rotational constant that was used. In the case of rotational tunneling, such an analysis is based on four possible overlap matrix elements, h_1, h_2, h_3 and h_4, and has already been performed very clearly by Punkkinen *et al* [12]. The very strong potentials around two of the threefold terahedral axes of NH_4 related to the so far unknown high-energy librational modes make our model with $h_3 = h_4 = 0$ and $h_1 \gg h_2$ a rather realistic one. A model with such parameters has already been discussed in [12] as being among the best ones. The overlap matrix elements are determined by the rotational potentials and thus by intermolecular interactions. To get reliable results, the shape of the three-dimensional wavefunction should be multiplied by a symmetry allowed polynomial to the simplest wavefunction, an isotropic Gaussian [44]. This procedure allows for significantly larger overlap/tunnel splittings, in the same way as the expression used above [43] for the one-dimensional case. Such forthcoming refinements are worth the effort only when the low-temperature crystal structure is known precisely to allow accompanying *ab initio* calculations. It also requires the interest and help of a real theorist.

5. Conclusion

The rotational potential of the NH_4^+ ion in ammonium persulfate is determined on the basis of librational modes and activation energies from this work and tunneling splittings and correlation times from the literature. Four different librational modes are identified by the isotope effect. They are consistent with the absence of symmetry at the ammonium site and the presence of one strong, one medium and two weak hydrogen bonds in agreement with x-ray diffraction [15]. In a one-dimensional model the heights of the corresponding four saddle points are found to differ by up to a factor of 4.7. A distinct lowest rotational barrier around the axis of a strong hydrogen bond leads to the dominance of the largest overlap tunneling matrix element, resulting in a single large tunnel splitting of the librational ground state of 1.09 μeV. On the basis of this observation, the ammonium dynamics was interpreted as a one-dimensional motion. This lowest barrier determines the classical rotational dynamics at low sample temperature. Quasi-elastic scattering follows, up to a sample temperatures $T \sim 100$ K, an Arrhenius dependence with an activation energy of 41 meV, which is too low for the lowest librational mode (17.3 meV) and the tunnel splitting of the ground state. A potential of dominant sixfold symmetry leads to a consistent description of all observed quantities and at the same time shows—again in agreement with experiment—an isotope effect which is largely reduced compared to the generally used harmonic description. Therefore the reduced isotope effect is a result of the special potential shape and not of changes in the properties of the hydrogen bond with deuteration. All results confirm, at the energy resolution of neutron spectroscopy, the model of one-dimensional reorientation of NH_4 molecules.

At temperatures $T \geqslant 140$ K, jumps across the second weakest barrier become visible and allow us to extract a second activation energy. A semi-quantitative analysis allows us a consistent description of this barrier with the next higher librational mode at 24.4 meV. The one-dimensional threefold potential that is in best agreement with observations contains a sixfold term of 10% amplitude. For NMR experiments [16] the dynamics about the two soft rotational barriers are already visible at the lowest temperatures as secondary tunnel splittings or slow jump dynamics. On the timescale of NMR—and similarly at the higher temperature in neutron spectroscopy—the ammonium rotation is, in a sense, two-dimensional or better bimodal.

Two new high-energy librational bands related to the remaining two threefold axes of rotation of the tetrahedron could be identified unambiguously by spectroscopy with high-energy neutrons. Barriers derived from the highest librational bands lead to a tunnel splitting of about 0.8 neV or a characteristic time of about 10^{-5} s. Such a process was observed by NMR in the partially deuterated sample but was wrongly attributed to changes in the intermolecular interactions with the appearance of dipolar moments in NH_3D^+. The rotational eigenmode with the highest energy and the longest characteristic correlation time are thus reconciled as fingerprints of the same dynamical behavior: rotation about the strongest axes. Thus all spectral features observed in ammonium persulfate are expression of a single dynamical process: three-dimensional rotation of the ammonium ion.

A methodological remark is necessary at the end: decomposing the problem of ammonium rotation into one-dimensional cuts through the three-dimensional potential is

helpful but cannot be quantitatively correct. An analysis of jump rotation analogous to the treatment of ammonium tunneling [12] as a three-dimensional process is desirable. The power of such a theory is that it will reconcile all observables in a common picture.

The need of a good single crystal shall be expressed here to attain the possibility of basing the actual phenomenological description by mathematical modeling on the fundamental intermolecular interactions. This is especially interesting in a hydrogen-bonded molecular crystal with an unusual shape of the rotational potential.

In summary, in the present work we have shown that all dynamical processes and excitations of the ammonium ion in $(NH_4)_2S_2O_8$ that are known so far can be fully explained by three-dimensional rotation in a very asymmetric tetrahedral potential with four axes of significantly different strengths.

Acknowledgments

We thank H Zimmermann of the Max-Planck Institute for Medical Research, Heidelberg, for supplying a deuterated ammoniumpersulfate single crystal. S Mattauch and A Loose participated for some time in an attempt to solve the low-temperature structure by single-crystal neutron diffraction. K Holderna-Natkaniec and V B Zlokazov analyzed the neutron powder diffraction spectra and refined the structural parameters at 20 K. M Russina and the Hahn-Meitner Institute, Berlin, are acknowledged for a test beam day at NEAT. The support on SPHERES by J Wuttke and discussions with W Press on various aspects of rotational tunneling are gratefully acknowledged.

References

[1] Hüller A and Kane J W 1974 *J. Chem. Phys.* **61** 3599
[2] Schlemper E O, Hamilton W C and Rush J J 1966 *J. Chem. Phys.* **44** 2499
[3] Rush J J, Zaylor T I and Havens W W 1960 *Phys. Rev. Lett.* **5** 507
[4] Bée M 1988 *Quasielastic Neutron Scattering* (Bristol: Hilger)
[5] Hüller A 1977 *Phys. Rev.* B **16** 1844
[6] Hüller A and Press W 1981 *Phys. Rev.* B **24** 17
[7] Press W 1981 *Single Particle Rotations in Molecular Crystals* (*Springer Tracts in Modern Physics* vol 81) (Berlin: Springer)
[8] Prager M and Heidemann A 1997 *Chem. Rev.* **97** 2933
[9] Prager M, David W I F and Ibberson R M 1991 *J. Chem. Phys.* **95** 2473
[10] Johnson M R and Kearley G J 2000 *Annu. Rev. Phys. Chem.* **51** 297
[11] Clough S, Horsewill A J, Johnson M R, Mohammed M A and Newton T 1991 *Chem. Phys.* **152** 343
[12] Kankaanpää M, Ylinen E E and Punkkinen M 2001 *Solid State Nucl. Magn. Reson.* **19** 19
[13] Kankaanpää M, Punkkinen M and Ylinen E E 2001 *Physica* B **305** 65
[14] Lalowicz Z T, McDowell C A and Ragunathan P 1978 *J. Chem. Phys.* **68** 852
[15] Schmidt T, Schmitt H, Zimmermann H, Haeberlen U, Lalowicz Z T, Olejniczak Z and Oeser T 2002 *Acta Crystallogr.* B **58** 760
[16] Olejniczak Z, Lalowicz Z T, Schmidt T, Zimmermann H, Haeberlen U and Schmitt H 2002 *J. Chem. Phys.* **116** 10343
[17] Olejniczak Z, Lalowicz Z T, Schmidt T, Zimmermann H, Haeberlen U and Schmitt H 2002 *J. Chem. Phys.* **117** 9808
[18] Schmidt T, Schmitt H, Haeberlen U, Olejniczak Z and Lalowicz Z T 2002 *J. Chem. Phys.* **117** 9818
[19] Lalowicz Z T, Punkkinen M, Vuorimäki A H, Ylinen E E, Detken A and Ingman L P 1997 *Solid State Nucl. Magn. Reson.* **8** 89
[20] Michel K H 1973 *J. Chem. Phys.* **58** 1143
[21] Töpler J, Richter D and Springer T 1978 *J. Chem. Phys.* **69** 3170
[22] Chesser N 1986 *Proc. Gatlinburg Conf. on Neutron Scattering*
[23] Sköld K 1968 *J. Chem. Phys.* **49** 2443
[24] Springer T 1977 *Dynamics of Solids and Liquids by Neutron Scattering* (*Topics in Current Physics* vol 3) ed S W Lovesey and T Springer (Berlin: Springer) p 284
[25] Squires G L 1978 *Introduction to The Theory of Thermal Neutron Scattering* (Cambridge: Cambridge University Press)
[26] Natkaniec I, Bragin S I, Brankowski J and Mayer J 1993 *Proc. ICANS-XIII, (Abingdon) RAL-Report 94-025* vol 1, p 89
[27] Prager M 2000 *Physica* **283** 376 http://www.fz-juelich.de/iff/Institute/ins/Broschuere_NSE/sv29.shtml
[28] http://www.fz-juelich.de/iff/Institute/ins/Broschuere_NSE/bss1.shtml
[29] http://www.jcns.info/jcns_spheres
[30] Lechner R E, Melzer R and Fitter J 1996 *Physica* B **226** 86
[31] http://www.frm2.tum.de/wissenschaft/spektrometer/tof-tof/index.html
[32] Unruh T, Neuhaus J and Petry W 2007 *Nucl. Instrum. Methods. Phys. Res.* A **580** 1414
[33] Zlokazov V B 2003 *Nucl. Instrum. Methods. Phys. Res.* A **502** 723
[34] Mattauch S, private communication
[35] Yamamuro O, Okishiro K, Matsuo T, Onoda-Yamamuro N, Oikawa K, Kamiyama T, Kume Y and Izumi F 1997 *J. Chem. Phys.* **107** 8004
[36] Weir R and Westrum E F Jr 1991 *J. Chem. Thermodyn.* **23** 653
[37] Swainson I P, Powell B M and Weir R D 1997 *J. Chem. Solid State Chem.* **131** 221
[38] Matsuo T, Kohno K, Inaba A, Mochida T, Izuoka A and Sugawara T 1998 *J. Chem. Phys.* **108** 9809
[39] O'Leary G P and Wheeler R G 1970 *Phys. Rev.* B **1** 4409
[40] Heidemann A, Anderson I, Prager M and Press W 1983 *Z. Phys.* B **51** 319
[41] Lister D G, MacDonald J N and Owen N L 1978 *Internal Rotation and Inversion* (London: Academic)
[42] Hecht K T and Dennison D M 1957 *J. Chem. Phys.* **26** 31
[43] Voll G and Hüller A 1988 *Can. J. Chem.* **66** 925
[44] Hüller A and Raich J 1979 *J. Chem. Phys.* **71** 3851